Relationships Between Atmospheric Stability and Near-Storm Turbulence

Johnathan D. Heaton[1,2], Stacey Hitchcock[3], and Cole Hartman[3]

[1]National Weather Center Research Experiences for Undergraduates Program
Norman, Oklahoma
[2]Metropolitan State University of Denver
Denver, Colorado
[2]School of Meteorology, University of Oklahoma
Norman, Oklahoma

ABSTRACT

Turbulence poses significant hazards to aircraft and contributes to substantial operational costs for commercial airlines. A substantial number of encounters occur near the tropopause while the plane is at cruise altitude (8-12 km), where the encounters are often linked to thunderstorm activity in the form of convectively induced turbulence (CIT). At this level, wind shear and static stability are the primary environmental characteristics that drive turbulence near thunderstorms. While the role of wind shear has been explored, the influence of atmospheric stability in the modulation of vertical and horizontal displacement of CIT remains less understood. This study gives particular attention to how turbulence in environments with different stability characteristics extends vertically above storm tops and horizontally by matching aircraft-based turbulence reports at cruise altitude with co-located ERA5 reanalysis dθ/dz grids from 2009 – 2014. The results from this study suggest that the increase of stability amplifies the distance over which the relative risk of encountering moderate or greater (MoG) turbulence remains elevated, especially below the tropopause.

1. INTRODUCTION

Turbulence is one of the most common hazards encountered by commercial aircraft, with events ranging from mild, routine disturbances to severe encounters that raise serious safety and operational concerns (Sharman et al. 2016). Significant turbulence can result in injuries to passengers and crew, structural damage to aircraft, and substantial operational costs to airlines. These costs often stem from delays, diversions, and increased fuel consumption due to turbulence avoidance maneuvers (Federal Aviation Administration 2006). Turbulence affecting aircraft occurs across a wide range of spatial scales, from meter-scale eddies that produce abrupt accelerations to kilometer-scale features that create broader, more persistent turbulent regions (Sharman et al. 2016). Turbulence arises in various forms, including mountain wave turbulence (MWT), clear-air turbulence (CAT), convectively induced turbulence (CIT), and wake turbulence from other aircraft (Sharman et al. 2016, Lane et al. 2012).

Among these types, CIT, which develops in and around convective clouds, presents unique challenges for forecasting due to its dependence on complex storm-environment interactions (Sharman et al. 2016). While convective regions are often highly turbulent, the risk of encountering moderate or greater (MoG) turbulence extends well beyond the storm itself. At horizontal distances up to 70 kilometers from convection, the likelihood of experiencing MoG turbulence is approximately twice the background risk (Hitchcock et al. 2025). This elevated likelihood is an example of relative risk, defined as the ratio of turbulence occurrence near storms to the baseline frequency. This approach provides a useful framework for quantifying how turbulence risk increases near convection (Lane et al. 2012, Hitchcock et al. 2025).

Advancing the understanding of CIT requires detailed observational data on turbulence occurrence and analysis of the near-storm environment in which it develops. Many past studies (e.g. Schwartz 1996; Gill 2016; Kim and Chun 2016; Miyamoto et al. 2023) have relied on pilot reports (PIREPs), which offer valuable insight into turbulence encounters and have been widely available over many years. However, PIREPs are subjective, vary in accuracy and resolution, and are unevenly distributed spatially and temporally due to their dependence on individual pilot perception and discretion (Schwartz 1996). Beyond pilot reports, remote sensing technologies offer an external lens for diagnosing convective structures and environmental conditions associated with turbulence. Radar and satellite observations provide broad spatial coverage and

help identify storm structures and convective features and offer important context for turbulence analysis (Lane et al. 2012). However, while turbulence can be derived from radar data, these remote sensing tools cannot directly detect turbulence as the spatial resolution is often too coarse to resolve the small-scale features responsible for turbulence near storms (Sharman et al. 2016). Because radar and satellite data cannot directly detect turbulence and current operational and onboard radars rely on the presence of precipitation, products derived from in-situ observations enable calculation of turbulence intensity based on the eddy dissipation rate (EDR). The use of EDR data allows for objective, quantitative assessments of turbulence intensity along flight tracks (Wingrove and Bach 1985; Cornman et al. 1995; Cornman et al. 2004; Sharman et al. 2014; Cornman 2016). While EDR data is limited to flight corridors (Fig. 1), it allows for more robust and comprehensive analyses of turbulence. One recent example of leveraging EDR data for the analysis of turbulence near storms is presented by Hitchcock et al. (2025), who quantified spatial risk gradients by comparing peak EDR intensity to convective features in radar reflectivity.

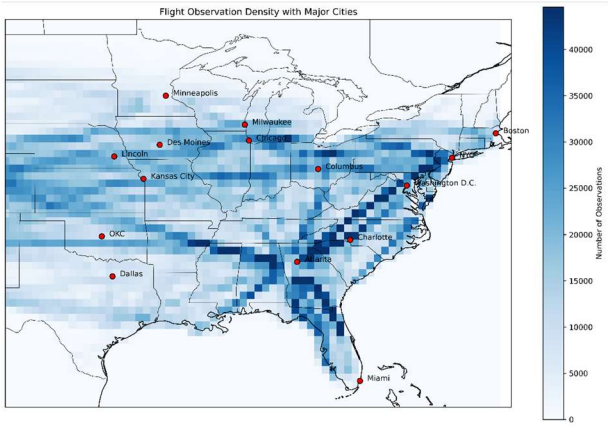

Figure 1: Flight observation density (shading) with major cities. Courtesy of Cole Hartman, used with permission.

CIT often arises near the tropopause, where strong vertical wind shear and enhanced static stability coexist. The tropopause serves as a strong stable layer that shapes the vertical development of clouds and influences the evolution of disturbances near the storm top (Tinney et al. 2022). When convection penetrates or distorts the tropopause, it can enhance horizontal wind shear and generate localized instabilities. The disturbance of the tropopause often leads to the formation of gravity waves above the overshooting convection, which often leads to the formation of gravity waves: buoyancy-driven oscillations that propagate through statically stable layers (Lane and Reeder 2001). Gravity waves produced by deep convection may travel vertically and horizontally into the upper troposphere and lower stratosphere (UTLS) (Trier and Sharman 2019). The growth of these gravity waves, combined with background shear, can lead to wave breaking in regions where the ratio of buoyant stability to vertical shear (referred to as the gradient Richardson number, Ri) is below 1 (Lane et al. 2012). Wave breaking can also occur in regions below a critical level where the wave speed is equal to the wind speed (Lane and Sharman 2008). When gravity waves break, they transfer energy into small-scale turbulent motions that can produce layers of turbulence far removed from the storm, particularly above or downstream (Fig. 2).

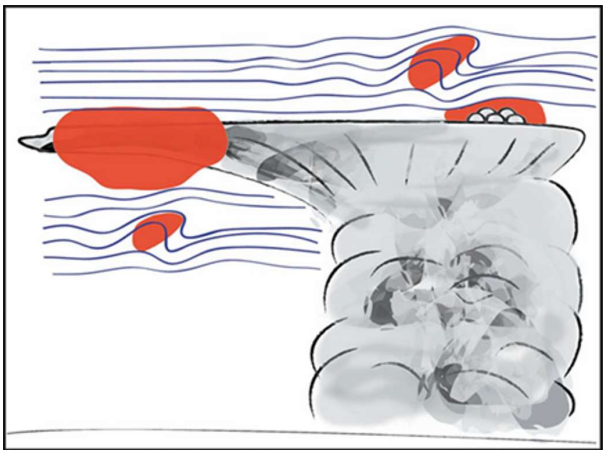

Figure 2: Diagram showing the regions of potential near-cloud turbulence (red shading) near a thunderstorm (grey shading). Black lines represent the cloud boundary, and blue lines represent isentropes (from Lane et al. 2012). Regions include the area underneath the anvil, mammatus clouds in the anvil, the area of overshooting convection, and the area above the overshooting convection.

Recent work (e.g. Hartman et al. 2026, unpublished manuscript; Hitchcock et al. 2025) suggests that the risk of turbulence above convection Is elevated during winter, especially in environments with strong winds and colder temperatures. However, this data alone does not provide sufficient information about the shear and stability structures that drive these elevated risks. A better understanding of the interaction between convection and the near-storm environment is

necessary to improve identification of hazardous turbulence in the UTLS.

Despite progress in understanding and detection of near-storm turbulence, forecasting turbulence near convection remains a challenge. Limitations in model resolution, gravity wave representation, and real-time observational data continue to constrain the ability to detect and predict CIT accurately in both operational and research contexts. Static stability is known to influence wave dynamics and the development of turbulence (Lane and Sharman 2008), but the relationship between stability and turbulence risk near thunderstorms has not been systematically quantified. To address this gap, this study uses ECMWF Reanalysis V5 (ERA5) reanalysis data (Hersbach et al. 2020) to evaluate how static stability varies across turbulence events in the vicinity of convection.

2. METHODS

Turbulence observations analyzed in this study are from a subset of the dataset described in Hitchcock et al. (2025) for the period between 2009 and 2014. The dataset includes aircraft-based measurements of EDR, which is recorded as the cube root of eddy dissipation rate ($m^{2/3}$ s^{-1}) and is derived from vertical wind or acceleration (Cornman et al. 1995, 2004; Cornman 2016, Hitchcock et al. 2025). Each automated report includes both the mean and peak EDR intensity over the previous minute, as well as the fractional timing (in tenths of a minute) of the peak value. Percentile thresholds are used to classify turbulence severity: Hitchcock et al. (2025) identified the 99.5th, 99.9th, and 99.99th percentiles of quality controlled EDR reports to be 0.16, 0.22, and 0.34 $m^{2/3}$ s^{-1}, respectfully. Values greater than each represent light or greater (LoG), moderate or greater (MoG), and severe or greater (SoG) turbulence, respectfully. The dataset of EDR data from commercial aircraft was manually filtered for data from cruise altitudes above 8 km and filtered for quality to retain only high-confidence reports (confidence greater than or equal to 0.9) with valid vertical wind data (for more information, see Cornman et al. 2004, Sharman et al. 2014, Cornman 2016, Hitchcock et al. 2025).

Storm context is provided by the GridRad v3.1 (Bowman and Homeyer 2022) composite radar product, which offers hourly 3D reflectivity fields on a 0.02° × 0.02° horizontal grid with 1 km vertical resolution up to 24 km AGL. Hitchcock et al. 2025 identified storm objects are identified as regions with coherent echo-top heights with embedded convection, and spatial metrics quantify turbulence report horizontal distances relative to the 10-dBZ boundary at the flight level and vertical distances from the echo top height (more details: see Hitchcock et al. 2025).

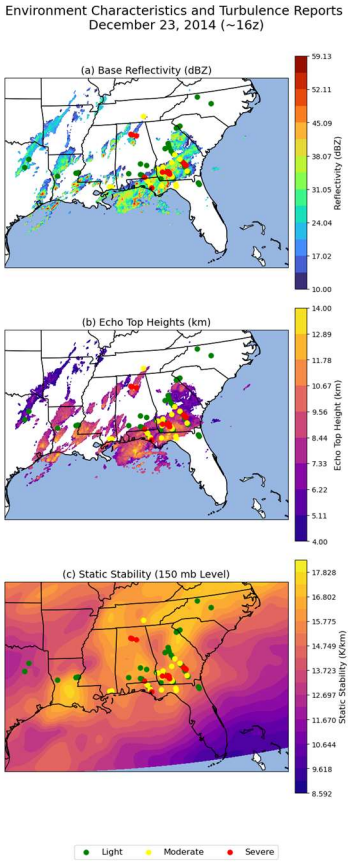

Figure 3: Turbulence Reports on December 23, 2014 (~16Z) overlayed with (a) GridRad reflectivity, (b) GridRad echo top heights, and (c) ERA5 static stability. For this figure, reports are limited to a ± 15-minute window around the top of each hour to align with radar imagery.Green, yellow, red dots show light, moderate, and severe EDR reports, respectively.

ERA5 reanalysis data (Hersbach et al. 2020), available hourly on a 0.25° x 0.25° horizontal grid with 37 vertical pressure levels, are used to characterize stability at the location of each EDR report. Following the calculation of θ and geopotential height, this study used the vertical gradient of potential temperature (dθ/dz) to assess static stability. For each EDR report, the nearest horizontal ERA5 grid point is identified using great-circle distance and temporal matching uses Xarray's "nearest" method (Hoyer and Hamman 2017). Then, because static stability

(dθ/dz) is calculated between pressure layers, it corresponds to approximate midpoints between standard pressure levels (e.g., 150 mb, 250 mb). The dθ/dz value from the matched grid cell and closest pressure level is assigned to each EDR report.

Reports with dθ/dz greater than or equal to 10 K/km are classified as occurring in strongly stable environments, which is a proxy for stratification typical near the tropopause (Tinney et al. 2022). At upper levels, the atmosphere is relatively dry, so it is reasonable to use the stratification criteria for dθ/dz values for dry air (Table 1), for this study. Nearly all of the near-storm environments analyzed in this study have dθ/dz values greater than 0 K/km; this study assesses the environment stability near each EDR report. For this study, dθ/dz greater than or equal to 10 K/km is considered above the tropopause consistent with Tinney et al. (2022).

Table 1: Stratification (dθ/dz) values of stability states of dry air.

Stability State (Dry Air)	Stratification
Absolutely Unstable	$\frac{\partial\theta}{\partial z} < 0$ K/km
Neutral	$\frac{\partial\theta}{\partial z} = 0$ K/km
Absolutely Stable	$\frac{\partial\theta}{\partial z} > 0$ K/km
Above the Tropopause (Tinney et al. 2022)	$\frac{\partial\theta}{\partial z} > 10$ K/km

The influence of static stability on turbulence occurrence near storms is assessed using relative risk, comparing MoG turbulence frequency (peak EDR greater than or equal to 0.22) within storm-proximity bins to the overall background frequency. Stability values are binned in 1 K/km increments from 1 – 22 K/km, with each bin containing all EDR observations that occurred in an environment within that stability range. For each bin, the risk is calculated as the frequency of observations in each bin with peak EDR greater than or equal to 0.22. This is compared to the background risk (0.00176), defined as the total number of MoG turbulence observations divided by the total number of observations in the full dataset. To avoid sensitivity to sparsely populated bins, relative risk values are excluded (set to NaN) for bins with less than 50 total observations.

3. RESULTS / ANALYSIS

Figure 4 captures distributions of dθ/dz for all EDR reports (Fig. 4a) and all MoG cases (Fig. 4b), irrespective of relative distance to convection. A consistent tendency toward lower static stability emerges in both subsets, with median values near 4.8 K/km and mean values near 6 K/km. Notably, a large proportion of reports fall within environments exhibiting 2 and 4 K/km and both subsets have the same mode of 3 K/km. These distributions diverge in slope, particularly on the right-hand side, implying a possible shift in stability within MoG report-prone environments. Figure 4 shows that aircraft often fly below the tropopause because more turbulence reports are in environments with dθ/dz less than 10 K/km. Given the differences in magnitude of reports in each subset, relative risk offers a more effective framework for identifying meaningful patterns in stability of the environments near MoG reports.

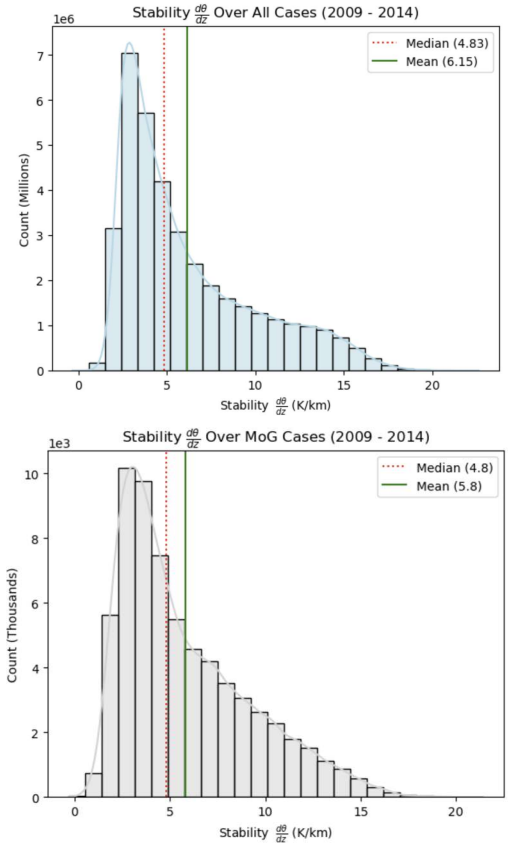

Figure 4: Distribution of stability over (a) all turbulence cases (blue) and (b) all MoG turbulence cases (grey), regardless of relative distance to convection.

Figure 5 shows the distribution of relative risk of MoG turbulence reports in each dθ/dz bin. Bins with relative risk greater than or equal to 1 denote that the risk of encountering MoG turbulence in that bin is greater than the background risk. Two red circles identify the stratification bins that meet this criteria: one circle with low stability (0 – 1 K/km) and one circle with dθ/dz bins between 6 – 10 K/km. Above the tropopause (dθ/dz greater than or equal to 10 K/km), relative risk is less than 1, which suggests that areas with stability greater than that of the tropopause have in general less risk.

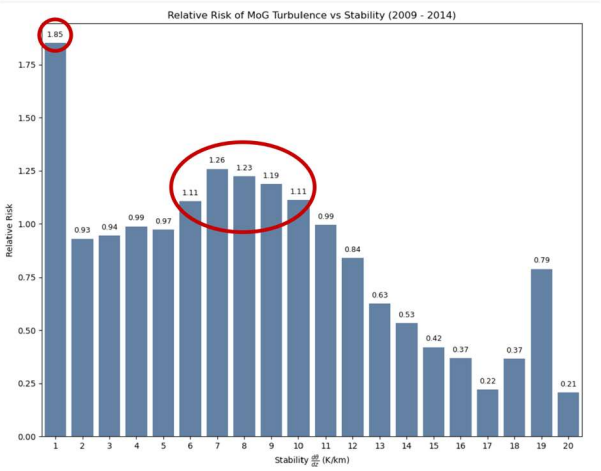

Figure 4: Relative Risk of MoG turbulence (x-axis) vs stability bins (y-axis). Red circles denote stability bins with relative risk greater than or equal to 1.

Risk can also be examined as a function of location relative to different parts of a storm. At vertical distances less than 0 km, where reports are located below echo top heights, relative risk increases with increases in stability (Fig. 6). The risk escalates sharply after 10 K/km and reaches over 50 times the background risk near 12 K/km. Between 0 and 1 km above a thunderstorm, relative risk increases with stability but remains lower than the risk within the echo top height. At 2 km above a thunderstorm, risk increases with stability then plateaus around 20 times the baseline from 2 – 16 K/km. Risk is still approximately 10 times the background level at 4 km above a thunderstorm and remains over twice the background level at 8 km above a thunderstorm. The trends of relative risk as a function of vertical distance suggest that elevated turbulence risk persists even well above storm tops.

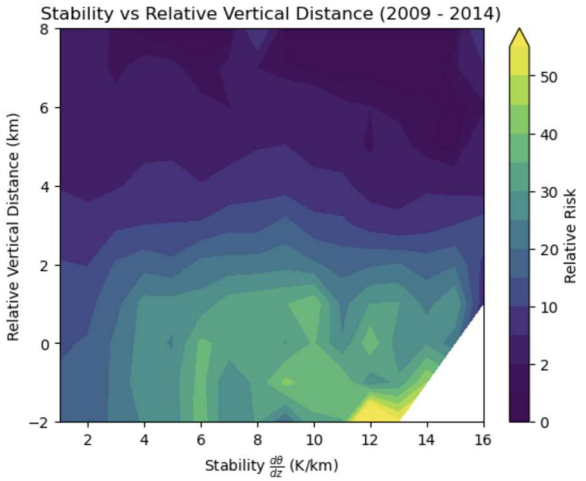

Figure 5: Relative risk (shaded) as a function of stability (x-axis) and relative vertical distance (y-axis) above a thunderstorm. Negative vertical distance values indicate reports from an aircraft below echo top height.

At any given stability level, relative risk of MoG turbulence encounters generally decreases with increasing vertical distance above a thunderstorm (Fig. 6). However, this vertical gradient is strongly modulated by the stability itself. For example, at higher stability values such as 12 K/km, relative risk begins at an elevated level (greater than 50 times the background) near the storm core and decreases sharply with altitude. In contrast, at lower stability values around 2 K/km, the risk is lower and decreases more slowly with vertical distance. Notably, risk values well within the storm in low-stability regimes are comparable to those observed approximately 2 km above the storm in highly stable conditions.

Generally, it can be noted that risk stability increases the risk of turbulence encounters at a distance from convection (Fig. 7) and that risk is higher inside a thunderstorm (where horizontal distance is less than or equal to 0 km, similar to Figure 6). For example, when stability is greater than or equal to ~8 K/km, at a horizontal distance of up to 70 km from a storm, the relative risk of encountering MoG turbulence is greater than ~10 times the background risk. At that same horizontal distance from a storm in an environment with lower stability (~4 K/km), the risk of a MoG turbulence encounter is ~5 times the background risk. Overall, Figure 7 suggests that flying in more stable conditions increases the chance of encountering MoG turbulence near thunderstorms, and that increasing stability increases the distance

over which risk remains elevated, especially below the tropopause.

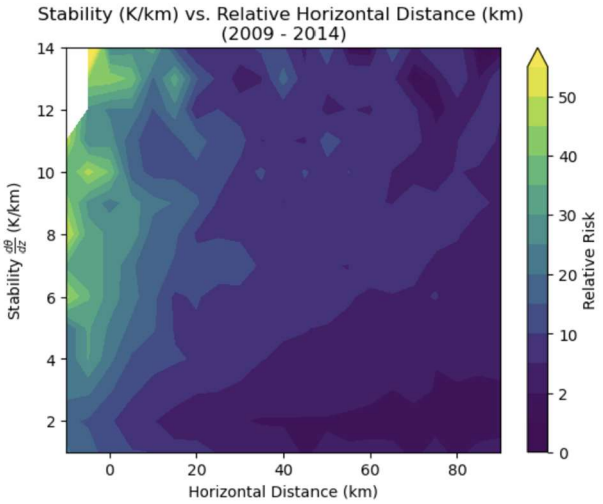

Figure 6: Relative risk (shaded) as a function of horizontal distance from 10-dBZ radar boundary (x-axis) and stability (y-axis).

4. DISCUSSION

4.1 *Limitations*

This analysis is subject to resolution-related constraints that may affect the interpretation of stability. ERA5 reanalysis data is hourly data, with a spatial resolution of 0.25° × 0.25°. Additionally, turbulence metrics derived from ERA5 were matched across only two pressure levels, separated by 100 mb. This limits its capacity to resolve smaller scale features within the near-storm environment. Consequently, convective structures such as overshooting convection, or fine-scale gradients and vertical features like tropopause folds may not be adequately represented. Therefore, computed potential temperature gradients broadly represent those of the background environment rather than the true stability at the location & time of the report.

Further, because relative risk is a ratio of ratios, there is interpretive complexity in regions of sparse sampling. Isolated bins may exhibit artificially elevated risk values due to low denominator counts rather than true physical enhancement. This was mitigated by requiring at least 50 total observations per bin, but localized points with significant differences from their surroundings should be interpreted cautiously. For example, a bin with dθ/dz ~8 K/km at a relative vertical distance of 8 km above a thunderstorm (Fig. 6) yielded disproportionately high risk estimates, likely reflecting statistical artifacts rather than realistic turbulence conditions.

4.2 *Stability Vs. Relative Vertical Distance*

Figure 6 shows a marked reduction in turbulence reports exceeding ~5 km above convective echo tops. Since deep convection often reaches ~8 – 15 km, a vertical separation of 5 km above the storm would place the aircraft beyond the certified ceiling for most commercial aircraft, which are limited by engineering and physiological constraints. For example, cabin pressurization systems are typically unable to sustain safe conditions above ~13.7 km AGL (FAA 2008).

Because aircraft cannot safely reach these heights, the reports observed at such large vertical separations likely occurred near storms with lower echo top heights. This scenario may be more common during the cold season, where tropopause levels are lower and convection tends to be shallower (Maddox and Mullendore 2018). The decrease in risk may reflect this seasonal shift rather than a purely spatial relationship.

To clarify these interpretations, future work should examine seasonal variations in echo top height alongside reported turbulence encounters. A more extensive dataset spanning more years would help characterize the role of environmental context in shaping the observed vertical risk pattern.

4.3 *Stability as a Modulator of Turbulence Displacement*

Observed increases in relative risk of MoG turbulence encounters at greater horizontal distances from thunderstorms under stable conditions suggest that static stability may play a primary role in redistributing turbulent energy (Fig. 7). One mechanism by which this occurs is gravity wave propagation. Thunderstorms can serve as potent gravity wave sources, and when these waves encounter stable layers, their vertical propagation is inhibited, allowing wave energy to travel horizontally across substantial distances (Lane and Sharman 2006).

5. Conclusion

This study analyzed the relationship between tropopause stability and CIT by focusing on MoG turbulence risk with relative distance to thunderstorms by matching ERA5 data spatially

and temporally with automated turbulence reports. The study finds that:

- Most reports (of any magnitude) come from the tropopause, and so occur in environments less stable than the tropopause.
- Environments with dθ/dz from 0 – 1 K/km and from 6 – 10 K/km have elevated risk for MoG turbulence encounters.
- As a function of stability, relative risk decreases at large vertical distances from a thunderstorm and increases at small vertical distances from a thunderstorm (or in a thunderstorm).
- Greater environmental static stability increases the chance of encountering turbulence generated by a thunderstorm, even if the storm is far away.

Together, these insights can help shape future turbulence avoidance efforts and support safer flight operations near convective environments.

6. ACKNOWLEDGMENTS

JH would like to thank the National Weather Center and the University of Oklahoma for making this research possible through the Research Experience for Undergraduates program. Gratitude goes to Stacey Hitchcock and Cole Hartman for their thoughtful mentorship and guidance throughout the project. Special thanks to Alex Marmo for opening the door for this REU opportunity, and to Daphne LaDue for her generous support, career advice, and help navigating the research world. JH also acknowledges Kathy Pegion for facilitating access to pre-downloaded ERA5 data. The authors appreciate Shawn Riley and Corey Coffey for maintaining the compute resources used, and airline companies who share the EDR data that helped make the analysis possible. This work was prepared by the authors with funding provided by National Science Foundation Grant No. AGS-2050267. The statements, findings, conclusions, and recommendations are those of the author(s) and do not necessarily reflect the views of the National Science Foundation.

7. REFERENCES

Bach, R. E., Jr., and R. C. Wingrove, 1985: Applications of state estimation in aircraft flight data analysis. J. Aircr., 22, 547-554.

Bowman, K., and C. Homeyer, 2017: GridRad - Three-Dimensional Gridded NEXRAD WSR-88D Radar Data. UCAR/NCAR - Research Data Archive, accessed 29 July 2025, https://doi.org/10.5065/D6NK3CR7.

Cornman, L. B., C. S. Morse, and G. Cunning, 1995: Real-time estimation of atmospheric turbulence severity from in-situ aircraft measurements. *Journal of Aircraft*, **32**, 171–177, https://doi.org/10.2514/3.46697.

Cornman, L.B., G. Meymaris, and M. Limber, 2004: An update on the FAA Aviation Weather Research Program's in situ turbulence measurement and reporting system. Preprints, 11th Conf. on Aviation, Range, and Aerospace Meteorology, Hyannis, MA, Amer. Meteor. Soc., 4.3.

Federal Aviation Administration, 2006: *Preventing Injuries Caused by Turbulence*. Advisory Circular 120-88A, U.S. Dept. of Transportation, 12 pp. [Available online at https://www.faa.gov/documentLibrary/media/Advisory_Circular/AC120-88A.pdf].

Federal Aviation Administration, 2008: *Pilot's Handbook of Aeronautical Knowledge*. FAA-H-8083-25A, U.S. Dept of Transportation, 490 pp. [Available online at https://www.faa.gov/regulations_policies/handbooks_manuals/aviation/pilot_handbook].

Gill, P. G., 2016: Aviation Turbulence Forecast Verification. *Aviation Turbulence: Processes, Detection, Prediction*, R. Sharman and T. Lane, Eds., Springer International Publishing, 261–283, https://doi.org/10.1007/978-3-319-23630-8_13.

Hartman, C., Hitchcock, S.M., 2025: A Climatology of Convectively Induced Turbulence (CIT) Over the United States. In preparation for *J. Appl. Meteor. Climatol.*

Hersbach, H., and Coauthors, 2020: The ERA5 global reanalysis. *Quart J Royal Meteoro*

Soc, **146**, 1999–2049, https://doi.org/10.1002/qj.3803.

Hitchcock, S. M., T. P. Lane, W. Deierling, R. D. Sharman, S. B. Trier, and C. R. Homeyer, 2025: Spatial Patterns of Turbulence near Thunderstorms. *Bulletin of the American Meteorological Society*, **106**, E1–E22, https://doi.org/10.1175/BAMS-D-23-0142.1.

Hoyer, S., and J. Hamman, 2017: xarray: N-D labeled Arrays and Datasets in Python. *JORS*, **5**, 10, https://doi.org/10.5334/jors.148.

Kim, S.-H., and H.-Y. Chun, 2016: Aviation turbulence encounters detected from aircraft observations: spatiotemporal characteristics and application to Korean Aviation Turbulence Guidance: Aviation turbulence encounters detected from aircraft observations. *Met. Apps*, **23**, 594–604, https://doi.org/10.1002/met.1581.

——, J.-H. Kim, H.-Y. Chun, and R. D. Sharman, 2023: Global response of upper-level aviation turbulence from various sources to climate change. *npj Clim Atmos Sci*, **6**, 92, https://doi.org/10.1038/s41612-023-00421-3.

Lane, T. P., and M. J. Reeder, 2001: Convectively Generated Gravity Waves and Their Effect on the Cloud Environment. *J. Atmos. Sci.*, **58**, 2427–2440, https://doi.org/10.1175/1520-0469(2001)058<2427:CGGWAT>2.0.CO;2.

——, and R.D. Sharman, 2006: Gravity Wave Breaking Above Deep Convection. *J. Atmos. Sci.*, **63**, 340—356, https://doi.org/10.1175/JAS3614.1.

——, and ——, 2008: Some Influences of Background Flow Conditions on the Generation of Turbulence due to Gravity Wave Breaking Above Deep Convection. *Journal of Applied Meteorology and Climatology*, **47**, 2777–2796, https://doi.org/10.1175/2008JAMC1787.1.

——, ——, S. B. Trier, R. G. Fovell, and J. K. Williams, 2012: Recent Advances in the Understanding of Near-Cloud Turbulence. *Bulletin of the American Meteorological Society*, **93**, 499–515, https://doi.org/10.1175/BAMS-D-11-00062.1.

Maddox, E.M., and G.L. Mullendore, 2018: Determination of Best Tropopause Definition for Convective Transpot Studies. *J. Atmos. Sci.,* **75**, 3361—3376, https://doi.org/10.1175/JAS-D-18-0032.1.

Miyamoto, Y., A. Matsumoto, and S. Ito, 2023: Statistical Analysis of Aviation Turbulence in the Middle–Upper Troposphere over Japan. *Journal of Applied Meteorology and Climatology*, **62**, 575–588, https://doi.org/10.1175/JAMC-D-21-0191.1.

NTSB, 2021: Preventing Turbulence-Related Injuries in Air Carrier Operations Conducted Under Title 14 Code of Federal Regulations Part 121.

Schwartz, B., 1996: The Quantitative Use of PIREPs in Developing Aviation Weather Guidance Products. *Wea. Forecasting*, **11**, 372–384, https://doi.org/10.1175/1520-0434(1996)011<0372:TQUOPI>2.0.CO;2.

Sharman, R., and T. Lane, eds., 2016: *Aviation Turbulence*. Springer International Publishing, https://doi.org/10.1007/978-3-319-23630-8.

Sharman, R. D., and S. B. Trier, 2019: Influences of Gravity Waves on Convectively Induced Turbulence (CIT): A Review. *Pure Appl. Geophys.*, **176**, 1923–1958, https://doi.org/10.1007/s00024-018-1849-2.

Sharman, R. D., L. B. Cornman, G. Meymaris, J. Pearson, and T. Farrar, 2014: Description and Derived Climatologies of Automated In Situ Eddy-Dissipation-Rate Reports of Atmospheric Turbulence. *Journal of Applied Meteorology and Climatology*, **53**, 1416–1432, https://doi.org/10.1175/JAMC-D-13-0329.1.

Tinney, E. N., C. R. Homeyer, L. Elizalde, D. F. Hurst, A. M. Thompson, R. M. Stauffer, H. Vömel, and H. B. Selkirk, 2022: A Modern Approach to a Stability-Based Definition of the Tropopause. *Monthly Weather Review*, **150**, 3151–3174, https://doi.org/10.1175/MWR-D-22-0174.1.

Trier, S. B., and R. D. Sharman, 2009: Convection-Permitting Simulations of the Environment Supporting Widespread Turbulence within the Upper-Level Outflow of a Mesoscale Convective System. *Monthly Weather Review*, **137**, 1972–1990, https://doi.org/10.1175/2008MWR2770.1.

——, and ——, 2018: Trapped Gravity Waves and Their Association with Turbulence in a Large Thunderstorm Anvil during PECAN. *Monthly Weather Review*, **146**, 3031–3052, https://doi.org/10.1175/MWR-D-18-0152.1.

ZoteroBib: Fast, free bibliography generator - MLA, APA, Chicago, Harvard citations,. Accessed 19 July 2025, https://zbib.org/.

Zovko-Rajak, D., and T. P. Lane, 2014: The Generation of Near-Cloud Turbulence in Idealized Simulations. *Journal of the Atmospheric Sciences*, **71**, 2430–2451, https://doi.org/10.1175/JAS-D-13-0346.1.